Chambers, J.E.; Wilkinson, P.B.; Wardrop, D.; Hameed, A.; Hill, I.; Jeffrey, C.; Loke, M.H.; Meldrum, P.I.; Kuras, O.; Cave, M.; Gunn, D.A.. 2012 Bedrock detection beneath river terrace deposits using three-dimensional electrical resistivity tomography. *Geomorphology*. ISSN: 0169-555X. 10.1016/j.geomorph.2012.03.034

Bedrock detection beneath river terrace deposits using three-dimensional electrical resistivity tomography

J.E. Chambers[a*], P.B. Wilkinson[a], D. Wardrop[b], A. Hameed[c], I. Hill[c], C. Jeffrey[c], M.H. Loke[d], P.I. Meldrum[a], O. Kuras[a], M. Cave[a], D.A. Gunn[a]

[a]*British Geological Survey, Environmental Science Centre, Nottingham, NG12 5GG, UK*

[b]*Lafarge Aggregates Ltd, Panshanger Park, Hertford, SG14 2NA, UK*

[c]*University of Leicester, Department of Geology, University Road, Leicester, LE1 7RH, UK*

[d]*Geotomo Software Sdn. Bhd., 115, Cangkat Minden Jalan 5, Minden Heights, 11700 Gelugor, Penang, Malaysia*

*Corresponding author. Tel.: +44(0)1159363428; Fax: +44(0)1159363261; E-mail: jecha@bgs.ac.uk.

Abstract

We describe the use of a fully volumetric geophysical imaging approach, three-dimensional electrical resistivity (3D ERT), for bedrock detection below mixed sand and gravel deposits typical of fluvial valley-fill terraces. We illustrate the method through an analysis of terrace deposits of the Great Ouse River (UK), where up to 4 m of sand and gravel have filled the valley bottom during the latest Pleistocene. We use an edge detector to identify the steepest gradient in first-derivative resistivity profiles, which yields an estimate of bedrock depth (verified by drilling) to a precision better than 0.2 m (average) and 0.4 m (standard deviation). Comparison of a range of drilling techniques at the site has revealed that borehole derived interface depths suffered from levels of uncertainty similar to those associated with the 3D ERT - indicating that the reliability of bedrock interface depths determined using these two approaches is comparable in this case. The 3D ERT method provides a high spatial resolution that enabled a previously unknown erosional bedrock structure, associated with the change from deeper first terrace to second terrace deposits, to be identified in the Great Ouse valley. The method provides a relatively quick method to quantify terrace fill volume over large sites to a greater degree of precision than currently available.

Keywords: river terrace; electrical resistivity tomography (3D); mineral exploration; image analysis; bedrock detection; three-dimensional

1. Introduction

River terrace deposits are a focus of considerable scientific, archaeological, and economic interest. Terrace architecture can provide important information regarding uplift, incision, and landscape evolution (e.g., Boreham et al., 2010; Bridgland, 2010), with the formation of aggradational terraces in some settings correlating closely with climatic cycles (e.g., Bridgland, 2006). These deposits are a particularly rich source of archaeological artefacts preserving a record of Palaeolithic human activity (e.g., Wymer, 1988) and are also a major economic resource of groundwater (Gomme and Buss, 2006) and sand and gravel aggregates for construction (Smith and Collis, 2001).

River terrace deposits can be highly variable and difficult to characterise in terms of structure and lithology, particularly where the deposits of multiple or dissected terraces are present (Gibbard, 1982; Peterson et al., 2011). Typical approaches to the characterisation of these deposits include geomorphological and geological mapping, remote sensing, and intrusive investigations (e.g., Suzuki et al., 2004; Guccione, 2008). Perhaps the most detailed and commonly undertaken subsurface investigations of river terrace deposits are for mineral exploration, where drilling is the principal investigative tool (Merritt, 1992; Crimes et al., 1994; Smith and Collis, 2001). However, because of the complexity of some deposits, even drilling using densely spaced boreholes can fail to adequately reveal the three-dimensional (3D) structure of a deposit in terms of thickness and composition (Wardrop, 1999).

To provide greater insights into subsurface heterogeneity, geophysical techniques such as seismic refraction, ground penetrating radar, and electrical methods are being increasingly applied (Hirsch et al., 2008; Tye et al., 2011). Electrical resistivity tomography (ERT) is one such method that has been demonstrated to be an effective means of studying the architecture of these deposits for a range of applications, including the investigation of landscape evolution (Froese et al., 2005; Hickin et al., 2009; Hsu et al., 2010), geological mapping (Tye et al., 2011), groundwater studies (Revil et al., 2005; Hirsch et al., 2008), and mineral exploration (Baines et al., 2002; Beresnev et al., 2002).

The principal benefits of ERT are that it provides high resolution images of the subsurface and is noninvasive. It is an effective means of characterising the subsurface because of the sensitivity of resistivity to variations in hydrogeological (e.g., saturation, pore fluid composition) and geological properties (e.g., mineral grain composition, porosity). In unconsolidated sediments, such as river terrace deposits, the major lithological control on resistivity is the type and proportion of clay minerals (Shevnin et al., 2007), with increasing clay content causing a decrease in resistivity.

Limitations of the technique include inaccuracies because of 3D structures to the side of the survey line or area and the indistinct appearance of boundaries resulting from the smoothness-constrained inversion techniques typically used for ERT imaging. Most previous ERT surveys of river terrace deposits have employed 2D, rather than 3D, imaging, because of its comparative rapidity and simplicity. However, for heterogeneous subsurface conditions, the two-dimensional (2D) assumption is violated because of the influence of 3D features in close proximity to the survey lines, which can cause significant inaccuracies in the resulting 2D resistivity models (Chambers et al., 2002; Sjodahl et al., 2006). More accurate subsurface reconstruction can therefore be achieved by applying fully 3D ERT imaging approaches. However, the smoothness-constrained images can make it difficult to accurately determine the position of geological boundaries, such as the river terrace deposit−bedrock interface. To address this problem, Hsu et al. (2010) described an automated approach to bedrock edge detection, although their study was restricted to 2D ERT. They provided both synthetic and field based examples with borehole control, both of which showed good visual agreement between the ERT derived interfaces and the known interface locations.

Here we present a study in which fully volumetric 3D ERT imaging is used to investigate river terraces from the Great Ouse valley, Bedfordshire, UK. The principal advance described here is the development and validation of an approach to bedrock surface detection in a river terrace setting based on 3D rather than 2D imaging. We propose that a fully volumetric approach is particularly preferable for highly variable deposits that have a fundamentally 3D structure. The specific aims of this study are (i) to quantitatively assess an automated approach to bedrock surface detection below highly heterogeneous valley fill deposits from the 3D resistivity model and (ii) to consider the respective merits of 3D ERT and conventional intrusive approaches for river terrace deposit characterisation.

2. Study area

The study area is located within the valley of the Great Ouse, near the village of Willington, 4 km to the east of Bedford, UK (Fig. 1). The Great Ouse is an important component of The Wash fluvial network, preserving a record of late Quaternary uplift and climate variation and of human activity during the Palaeolithic, and as such is of international significance (e.g., Boreham et al., 2010). The geology comprises Quaternary alluvium and river terrace sand and gravel overlying Oxford Clay Formation bedrock of the middle Jurassic (Barron et al., 2010). In this area the Oxford Clay bedrock consists of the Peterborough member, which is a brownish grey, fissile mudstone, with an approximate thickness of 20 m. The Oxford Clay outcrops to both the southeast and northwest of the survey area, and has been exposed by extractive activities within the river valley (Fig. 1). The river terrace deposits are of the Ouse Valley Formation and are likely to have been deposited by braided rivers under periglacial conditions during different Quaternary cold stages (Rogerson et al., 1992; Green et al., 1996; Bridgland, 2010). Three principal terrace deposits are observed in the area (Horton, 1970; Barron et al., 2010; Boreham et al., 2010). The first, and lowest, terrace overlies the Felmersham member, which is ~ 3 m thick, with a surface between 0.6 and 2 m above the floodplain. The second terrace overlies the Stoke Goldington member and has a surface hereabouts between 2 and 7 m above the floodplain. The third terrace overlies the Biddenham member, which has a thickness of up to 7 m and a surface between 11 and 13 m above the floodplain. The sands and gravels of the three terraces display a similar composition, comprising planar−bedded, brownish yellow sand and gravel for which the gravel component mainly consists of flint and limestone. The present day floodplain is covered by a brown clay and silt alluvium, with a thickness of up to 4 m, which overlies the Ouse Valley Formation and in places may occupy channels cut in the Felmersham member by meandering rivers under temperate climate conditions (Barron et al., 2010). Extensive removal and reworking of the superficial deposits in this area has occurred from mineral extraction and, in particular, the quarrying of sand and gravel from the river terrace deposits. In many places the removal of sand and gravel has resulted in the exposure of the Oxford Clay Formation bedrock (Fig. 1).

<Insert Fig. 1 near here>

The study site is situated on terrace deposits of the undifferentiated Felmersham and Stoke Goldington members (Fig. 1), overlying Oxford Clay Formation bedrock. The terrace deposits at this site are the focus of a long-standing sand and gravel operation. At the time of this study, the topsoil (which was ~ 0.2 m thick), had been stripped and banked (Fig. 2) exposing alluvium at the surface. The alluvial materials observed across the survey area are probably modern overbank deposits, which are distinct from the thicker alluvium recorded on the geological map (Fig. 1). The area was selected because good subsurface data in the form of borehole logs was available with which to interpret and calibrate the geophysical results. Furthermore, mineral extraction activities immediately to the south of the study site and electromagnetic geophysical reconnaissance surveys (Hill et al., 2011) had revealed that the river terrace deposits in this area were extremely variable in terms of thickness and composition, thereby providing a complex target with which to test 3D ERT. The deposits were unsaturated because of dewatering associated with the mineral workings immediately to the south of the study site (Fig. 2).

<Insert Fig. 2 near here>

3. Methodology

3.1. Intrusive investigations

Drilling at the site was carried out using a flight auger supplemented with holes drilled using other standard techniques, including shell and auger, reverse circulation, and sonic drilling. A total of 11 locations were drilled within the 3D ERT imaging area; five of the locations were drilled using only the flight auger; whilst the remaining six locations were drilled with a combination of two or more techniques. At each location bedrock was proven. For locations where multiple drilling techniques were applied, boreholes were drilled within ~ 1 m of one another. The drilling density achieved (i.e., about 11 holes per hectare) was considerably in excess of standard sand and gravel exploration drilling programmes that typically employ a 100-m drilling grid, which in complex situations can be reduced to 50 m. The drilling at the site was undertaken as a component of a separate project concerned with optimising sand and gravel deposit sampling strategies, which involved the geostatistical analysis of grading data and the comparison of different drilling technologies (Hill et al., 2011; Jeffrey et al., 2011). Although the borehole locations were selected principally for the purpose of undertaking geostatistical analysis of grain size variations, they nevertheless provided a useful ground truth data set with which to assess the performance of 3D ERT for river terrace deposit characterisation and bedrock detection. Borehole locations are shown in Fig. 2, and summary information showing depth to bedrock determined by drilling is shown in Table 1.

<Insert Table 1 near here>

3.2. Electrical resistivity tomography

The application of ERT can provide fully 3D volumetric models of subsurface resistivity distributions from which features of contrasting resistivity can be located and characterised. Methodologies for 3D data collection and modelling are well established in the literature (e.g., Chambers et al., 2007, 2011; Magnusson et al., 2010) and so only a brief summary is presented here.

3.2.1. Survey design and execution

The 3D ERT survey was carried out within an area of 93 m (x) by 93 m (y). Data were collected on a network of 32 orthogonal survey lines positioned at 6-m intervals, oriented in both x and y directions (Fig. 2). The dipole-dipole array with dipole sizes (a) of 3 and 6 m, and dipole separations (n) of 1a to 8a were used, and a full set of both normal and reciprocal measurements were collected. A line separation twice that of the along-line electrode separation was selected to avoid undersampling and to maximise survey coverage rate (Gharibi and Bentley, 2005). Likewise, the selected dipole sizes and separation were considered to be a reasonable compromise between vertical and lateral resolution and coverage rate. Orthogonal lines were employed to minimise bias in the resulting ERT model resulting from the use of a single line direction (Chambers et al., 2002). The dipole-dipole array was used because it is a well-tested array that can provide a relatively high level of resolution, it does not require a remote electrode, it can exploit the multichannel capabilities of modern ERT instruments, and crucially, it enables the efficient collection of reciprocal measurements (Dahlin and Zhou, 2004). For a normal four-electrode measurement of transfer resistance, the reciprocal is found by exchanging the current and potential dipoles, and in the absence of nonlinear effects should give the same result. Here, reciprocal error is defined as the percentage difference between the forward and reciprocal measurement. Reciprocal measurements are sensitive to both random and systematic sources of noise, and provide a particularly effective means of assessing data quality and determining robust data editing criteria (Dahlin and Zhou, 2004).

A real-time kinematic global positioning system (GPS) survey was undertaken to measure surface elevations across the area for incorporation into the resistivity inversion and forward modelling procedure. Although most of the survey area was very flat, the GPS survey was required to capture the topography of a 3-m-high bank of topsoil that encroached on the eastern corner of the ERT imaging area (Fig. 2).

3.2.2. Data processing, forward modelling, and inversion

The combined data set from the survey lines comprised 11,270 pairs of normal and reciprocal measurements. In general, data quality diminished with increasing geometric factors, which cause smaller measured potential differences. Data points with a reciprocal error of > 5% were removed, which in this case accounted for only 2% of the measured data, resulting in a filtered data set of 10,952 pairs. These were inverted using a 3D regularized least-squares optimization method (Loke and Barker, 1996). The forward problem was solved using the finite-element method, in which node positions were adjusted to allow topography to be taken into account in the inversion process. In brief, the aim of the inversion process is to calculate a model that satisfies the observed data. A starting model is produced, which in this study was a homogeneous half-space, for which a response is calculated and compared to the measured data. The starting model is then modified in such a way as to reduce the differences between the model response and the measured data; these differences are quantified as a mean absolute misfit error value. This process continues iteratively until acceptable convergence between the calculated and measured data is achieved. In this case, a geologically realistic model was produced using L2-norm (smooth) model constraints because of the significant gradational lithological variations observed in the drift deposits and the undulating topography of bedrock (Loke et al., 2003). The final resistivity model consisted of 31 cells in the *x*-direction, 31 cells in the *y*-direction, and 11 layers in the *z*-direction, resulting in a total of 10,571 model cells.

3.2.3. Bedrock detection

Amongst the most widely used approaches to edge detection are gradient techniques, which assume interfaces are located where changes in image properties are at a maximum (e.g., Marr and Hildreth, 1980; Vafidis et al., 2005; Sass, 2007). One of the only published examples of automated bedrock detection from ERT images is described by Hsu et al. (2010). They used a gradient method, which searches for values of zero in the Laplacian (second derivate) of the resistivity image in the horizontal and the vertical directions. Using this approach, they were able to accurately define the bedrock-sediment interface from a number of 2D ERT images. The principal drawback of the Laplacian technique was, according to their study, the prevalence of local zero lines that were difficult to differentiate from those associated with the larger magnitude gradients defining the primary bedrock interfaces.

Here we adopt a similar technique to Hsu et al. (2010). However, because of the added complexity of 3D image analysis compared to 2D, we have simplified their approach. We only consider variation in gradient in the vertical direction that although is less sensitive to very steeply dipping or vertical interfaces, is a reasonable approximation for the relatively layered structure of the river terrace deposits. We also only consider the gradient (first derivative) of the resistivity image, which tends to reduce the problem of the Laplacian method, which produces many more *false* interface (zero) lines. Although the first derivative eliminates false interfaces, it cannot discriminate between interfaces if multiple gradients are present.

Consequently, we employ a two-stage heuristic approach for bedrock detection at the study site. First, if multiple gradients in the correct direction (i.e., decreasing resistivity with decreasing elevation) are present then the steepest gradient is chosen; this is because we anticipate that in most cases the steepest resistivity gradient in the subsurface will be between the relatively coarse-grained river terrace deposits and very clay rich Oxford Clay, rather than lithological boundaries within formations or between the alluvium and terrace deposits. Second, if the gradients are of a similar magnitude, we pick the deeper gradient, as the lower lithological interface in the ERT model is likely to be between the valley fill and bedrock surface.

Our implementation of the steepest gradient method involved extracting resistivity data, ρ, as a function of elevation, z, for each surface position (x, y). An interpolating curve was fitted through $\rho(z)$ for each (x, y) point. In this case, a piecewise cubic hermite interpolating polynomial (PCHIP) was used. The coefficients of the polynomial are chosen so that the resistivity is continuous and smooth, its first derivative is continuous (although not necessarily smooth), and the interpolant is monotonic between data points (e.g., Fig. 3). This has the effect that the interpolant preserves the shape of the data (Fritsch and Carlson, 1980). Once the coefficients are determined, the first derivative can be calculated analytically. Then for interface detection, the depth corresponding to the steepest gradient on the interpolating curve that satisfied our heuristic was identified for each (x, y) point.

<Insert Fig. 3 near here>

4. Results and discussion

4.1. Direct intrusive sampling

The drilling results for the 11 locations (Fig. 2) in terms of the types of drilling techniques deployed, position, ground level, and depth to bedrock are shown in Table 1. The average depth to bedrock from each location, and hence river terrace and alluvium thickness, ranges from 2.1 to 4.2 m. Significant differences in deposit thickness were observed between the various drilling techniques for each location. The alluvium showed a consistent thickness of ~ 1 m across the survey area. Bedrock interface depths determined by multiple holes were not consistent (Table 1); the discrepancies ranged between 0.2 and 1 m, with an average of 0.46 m. The reasons for this apparent lack of agreement between drilling techniques are threefold: first, misidentification of interfaces because of contamination by material from the hole sides during stem withdrawal (a problem that is recognised in the interpretation of flight auger logging in particular); second, poor core recovery and slippage of core in the barrel during withdrawal (as observed to occur with, for example, sonic drilling); and third, true variation in bedrock surface elevation between clustered sampling points (i.e., ~ 1 m separation).

4.2. Three-dimensional resistivity model

Good convergence between the observed and model data was achieved, as indicated by the mean absolute misfit error of 2.4%. The resulting resistivity model has dimensions of 93 m (*x*) by 93 m (*y*) and extends to a depth of 14 m below ground level (*z*). Visualisations of the 3D ERT model are shown in Fig. 4 as a series of vertical and horizontal sections and volumetric images. The clay bedrock is defined as low resistivity material underlying more resistive and highly heterogeneous valley fill deposits. The banked topsoil in the eastern corner displays a similar resistivity range to that of the terrace deposits.

<Insert Fig. 4 near here>

The distribution of inverted resistivities is shown in Fig. 5, plotted as a probability density function (PDF). The PDF was estimated using a kernel smoothing algorithm (Sheather and Jones, 1991), which sets up a normal distribution at each of the measured values in the data set and adds these together to produce smoothed PDF. Using the standard deviation (SD) and relative proportions of points from an initial approximation as starting points, an optimisation routine (Rowan, 1990) that modifies the input parameters to minimise the root mean square error between the estimated PDF and the actual PDF was used to determine mean and standard deviations for each of the predicted resistivity populations. Three resistivity populations with means of 15, 60, and 125 Ωm, respectively, were estimated using this approach. The well-defined low resistivity peak (peak 1) corresponds to the Oxford Clay bedrock, whilst the higher resistivity and less distinct peaks are consistent with separate populations within the deposits of varying composition. For unsaturated valley fill deposits present at this site, the high resistivity population (peak 3) is likely to be associated with relatively clean coarse sand and gravel, whilst the lower resistivities (peak 2) are consistent with the more clay-rich alluvium.

<Insert Fig. 5 near here>

The geological sequence at the site — comprising a thin layer of alluvium at the surface, river terrace sand and gravel, and Oxford Clay bedrock — is apparent in the 3D ERT image (Fig. 4). The alluvium is seen as a thin layer of relatively low resistivity (< 100 Ωm) material (e.g., Figs. 4 and 6), which indicates a higher clay content than the underlying sand and gravel. The alluvium appears to vary in composition across the area, with the northwestern corner and southern edge showing a higher resistivity, due perhaps to a lower clay content. The underlying terrace deposits are generally more resistive than both the alluvium and the Oxford Clay bedrock. They display a broad range of resistivities with a spatial distribution that is consistent with deposition as part of a braided river system, with silt and clay-rich channel fill and coarser bar deposits. The Oxford Clay bedrock is associated with a relatively homogeneous resistivity distribution. A number of slightly higher resistivity zones are seen within the bedrock, with the two strongest features at $y = 0$ m and $x = 25$ and 75 m, respectively. It is probable that these are artefacts of the inversion process rather than real bedrock features for three principal reasons. First, they are not consistent with known geological structure. Second, they are in a part of the model that has low model resolution (Wilkinson et al., 2012); in this case the model resolution reduces by more than an order of magnitude between 4 m below ground level and the base. Third, because they are at the base of the model they are influenced by measurements with higher geometric factors, which have poorer signal-to-noise characteristics.

<Insert Fig. 6 near here>

The primary structure is an arch-shaped feature (Fig. 4), running approximately SW to NE, which defines thicker terrace deposits and deeper bedrock to the NW. The transition from thicker to thinner deposits is likely to represent that transition from first to second terrace. Three lines of evidence corroborate this interpretation. First, it is close to the anticipated transition between the first and second terrace (Barron et al., 2010; A.J.M. Barron, British Geological Survey, personal communication, 2011). Second, the thickness and height change between the first and second terraces recorded in the area (Horton, 1970; Barron et al., 2010; Boreham et al., 2010) are consistent with the structure observed in the ERT model. Third, the orientation of the erosional structure identified in the ERT model is subparallel to the long axis of the Great Ouse.

4.3. Steepest gradient method bedrock surface detection

The bedrock surface extracted from the 3D ERT model using the steepest gradient (first derivative) method extends between 20 and 24 m above Ordnance Datum (AOD) (Fig. 7). The broad structure identified in the 3D ERT model, interpreted as the transition from first to second terrace, is clearly visible in the steepest gradient bedrock surface as a sharp upward step toward the eastern corner of the image. In addition, the steepest-gradient–derived surface contains a scattering of false high elevation points where our heuristic approach failed to capture the full complexity of resistivity variations in the model. These points appear as isolated spikes, or bull's-eyes, and are concentrated in the northwestern corner, below the higher resistivity alluvium, and in the southeastern corner, below the topsoil bank.

<Insert Fig. 7 near here>

Examples of interpolated resistivity depth curves from the 3D ERT model, showing the location of the steepest gradient and 'known interface' resistivities, are given for borehole locations 11 and 15 (Fig. 6). The known interface resistivity is the value associated with the borehole-defined depth; an alternative to the steepest gradient approach is to use the known interface resistivity to define an isoresistivity surface, which is assumed to coincide with the bedrock surface (see discussion on the use of isoresistivity surfaces below). Summary data for each of the borehole locations is given in Table 2. Statistical analysis has been carried out using the Bland and Altman (1986) method, which provides a means of comparing two different methods of measurement (i.e., ERT and boreholes) where the true value of the measured parameter is unknown. It is used to calculate the bias and the agreement, or standard deviation, between the two methods. This approach has indicated a reasonable agreement between the boreholes and steepest-gradient–derived method as indicated by an SD of 0.38 m (Fig. 8A). A slight bias of 0.19 m caused by two outlying data points (BH8 and BH13) has been observed between the boreholes and steepest gradient method, with the ERT-derived bedrock elevations slightly higher than those recorded in the boreholes. Likewise, the Pearson correlation coefficient for the steepest gradient and borehole-derived bedrock elevations is 0.83, with a p-value of 0.001 (Fig. 8B), indicating good agreement between the two approaches and a high degree of statistical significance. Based on the steepest gradient method, a volume of 12,250 m^3 (SD 3240 m^3) has been calculated (using the trapezoidal rule) for the valley fill sediment (terrace sand and gravel, and alluvium) within the 3D ERT survey area.

<Insert Table 2 near here>

<Insert Fig. 8 near here>

These results also confirm the findings of Hsu et al. (2010) that isoresistivity lines are not necessarily a good indicator of bedrock surface geometry. For isoresistivity lines to successfully define the bedrock surface, the interface must be characterised by a consistent value of resistivity. By comparing the results of the 11 drilling locations with the ERT model, it is clear that the range of interface resistivity values is considerable (Table 2), varying between 42 and 520 Ωm. The large range of interface resistivities is a function of the complexity of the deposit, with the valley fill deposits displaying a large resistivity range and significant heterogeneity. This is further illustrated with reference to Fig. 6, where the interface resistivity for BH 11 is 520 Ωm, whilst for BH15 it is 280 Ωm. The reason for the difference between these two locations is that at BH11 the terrace deposits were significantly more resistive than at BH15, resulting in a large difference in interface resistivity values.

4.4. Comparison of 3D ERT and borehole results

Drilling and ERT produce very strongly contrasting types of information. Boreholes provide very detailed, very high resolution (centimetre to decimetre scale) information for vertical profiles at discrete locations but provide very poor lateral resolution, even for dense drilling grids or profiles considered here, because of separations that are typically on the scale of at least tens of metres between holes. Moreover, drilling can provide direct samples of subsurface materials. Conversely, 3D ERT provides high resolution (metre scale) spatially continuous volumetric subsurface models but provides indirect information on material properties. Interestingly, the uncertainty associated with bedrock surface elevation for both drilling and ERT was of a similar magnitude (i.e., tens of centimetres), with an average discrepancy between drilling techniques of 0.46 m (section 4.1) and a standard deviation of 0.38 m for the difference between steepest gradient and average borehole-derived bedrock elevations (section 4.3).

In this geological setting, the spatial information provided by ERT was essential for resolving the structure of the bedrock surface, due the complexity of the deposit, in terms of thickness variations and sediment heterogeneity. The relative success of ERT was a function of the spatial resolution (in the *x*-, *y*- and *z*-directions) of the technique, which was closer to the scale of deposit heterogeneity than the borehole data, which had sufficient resolution only in the *z*-direction. However, intrusive investigations and sampling will always be necessary for this type of investigation, whether it be for mineralogical assessment and dating for geological, geomorphological, or archaeological studies; hydrogeological testing for groundwater resource assessment; or particle size distribution determination for mineral exploration. Crucially, intrusive sampling is also essential for the calibration and validation of geophysical images. These two approaches are therefore complementary. The combined use of 3D ERT and boreholes has the potential to reduce the number of boreholes required, and the ERT images could also assist in the more effective targeting of boreholes.

Boreholes were also important for deposit characterisation in this case, as they were able to differentiate between river terrace and alluvium. The 3D ERT model did reveal a thin, relatively conductive layer across much of the surface of the model, but in places alluvium was indistinguishable from the underlying sand and gravel due to insufficient resistivity contrasts (e.g., Figs. 4 and 5). For this reason the steepest gradient method was not applied to identify the interface between the alluvium and the sand and gravel.

5. Conclusions

Automated bedrock detection from 3D ERT imaging at a site in the Great Ouse Valley, UK, using the steepest gradient (first derivative) method was shown to correlate well with borehole-derived bedrock elevations. Comparison of the borehole and steepest gradient methods has enabled the performance of 3D ERT for bedrock detection to be quantitatively assessed and uncertainty associated with sediment volume calculations to be determined. Whilst the steepest gradient method was shown to provide a good quality bedrock elevation model, isoresistivity lines were shown to provide a very poor indication of bedrock rock surface depth and geometry in this situation. Interestingly, a comparison of a range of drilling techniques deployed at the site has indicated a level of uncertainty for borehole derived interface depths similar to that associated with 3D ERT steepest gradient edge detection – indicating that intrusive sampling cannot always be regarded as providing inherently more reliable information than geophysical investigations.

Subsurface geological variations (including the distribution of major formations, and lithological heterogeneity, and river terrace deposit thicknesses) were captured within the 3D ERT model. Crucially, a major erosional feature on the bedrock surface was identified as the boundary between first and second terrace deposits of the Great Ouse valley.

Three-dimensional ERT image analysis using the steepest gradient method has been shown to be an effective bedrock detection method in this locality, owing in part to the strong contrast in resistivity between the bedrock and river terrace deposits. It is therefore reasonable to presuppose that ERT would be similarly successful in other river terrace settings with strong resistivity contrasts between valley fill and bedrock materials. In particular, in areas of clay or mudstone bedrock, a good resistivity contrast could be expected with river terrace sand and gravel because of the large difference in the proportion of clay between the two material types.

The appropriateness of 3D ERT for any given setting will also be dependent on a number of other factors, including the required spatial coverage and level of resolution. The practical limit of survey coverage using 3D ERT is probably in the order of a few tens of hectares for individual surveys and, as such, is not equivalent to surface mapping approaches using remote sensing or towed ground-based systems that permit very rapid large-scale data collection. Therefore, in the context of river terrace deposit investigations, 3D ERT is best suited to targeted site-specific surveys associated with complex deposits displaying significant lateral variations where detailed information on subsurface structure is required.

Acknowledgements

The research was funded by Defra through the MIST Programme (Grant MA/7/G/1/007) and in-kind contributions from project partners. This paper is published with the permission of the Executive Director of the British Geological Survey (NERC). The authors wish to thank A.J.M. Barron for his advice on the local geology.

References

Baines, D., Smith, D.G., Froese, D.G., Bauman, P., Nimeck, G., 2002. Electrical resistivity ground imaging (ERGI): a new tool for mapping the lithology and geometry of channel-belts and valley- fills. Sedimentology 49, 441-449.

Barron, A.J.M., Sumbler, M.G., Morigi, A.N., Reeves, H.J., Benham, A.J., Entwisle, D.C., Gale, I.N., 2010. Geology of the Bedford District - A Brief Explanation of the Geological Map. 1:50 000 Sheet 203 Bedford (England and Wales), Nottingham.

Beresnev, I.A., Hruby, C.E., Davis, C.A., 2002. The use of multi-electrode resistivity imaging in gravel prospecting. Journal of Applied Geophysics 49, 245-254.

Bland J.M., Altman D.G., 1986. Statistical methods for assessing agreement between two methods of clinical measurement. Lancet, i, 307-310.

Boreham, S., White, T.S., Bridgland, D.R., Howard, A.J., White, M.J., 2010. The Quaternary history of the Wash fluvial network, UK. Proceedings of the Geologists Association 121, 393-409.

Bridgland, D.R., 2006. The Middle and Upper Pleistocene sequence in the lower Thames: a record of Milankovitch climatic fluctuation and early human occupation of southern Britain - Henry Stopes Memorial Lecture 2004. Proceedings of the Geologists Association 117, 281-305.

Bridgland, D.R., 2010. The record from British Quaternary river systems within the context of global fluvial archives. Journal of Quaternary Science 25, 433-446.

Chambers, J.E., Ogilvy, R.D., Kuras, O., Cripps, J.C., Meldrum, P.I., 2002. 3D electrical imaging of known targets at a controlled environmental test site. Environmental Geology 41, 690-704.

Chambers, J.E., Wilkinson, P.B., Weller, A.L., Meldrum, P.I., Gilvy, R.D., Caunt, S., 2007. Mineshaft imaging using surface and crosshole 3D electrical resistivity tomography: a case history from the East Pennine Coalfield, UK. Journal of Applied Geophysics 62, 324-337.

Chambers, J.E., Wilkinson, P.B., Kuras, O., Ford, J.R., Gunn, D.A., Meldrum, P.I., Pennington, C.V.L., Weller, A.L., Hobbs, P.R.N., Ogilvy, R.D., 2011. Three-dimensional geophysical anatomy of an active landslide in Lias Group mudrocks, Cleveland basin, UK. Geomorphology 125, 472-484.

Crimes, T.P., Chester, D.K., Hunt, N.C., Lucas, G.R., Mussett, A.E., Thomas, G.S.P., Thompson, A., 1994. Techniques used in aggregate resource analyses of 4 areas in the UK. Quarterly Journal of Engineering Geology 27, 165-192.

Dahlin, T., Zhou, B., 2004. A numerical comparison of 2D resistivity imaging with 10 electrode arrays. Geophysical Prospecting 52, 379-398.

Fritsch, F.N., Carlson, R.E., 1980. Monotone Piecewise Cubic Interpolation. SIAM J. Numerical Analysis 17, 238-246.

Froese, D.G., Smith, D.G., Clement, D.T., 2005. Characterizing large river history with shallow geophysics: middle Yukon River, Yukon Territory and Alaska. Geomorphology 67, 391-406.

Gharibi, M., Bentley, L.R., 2005. Resolution of 3-D electrical resistivity images from inversions of 2-D orthogonal lines. Journal of Environmental and Engineering Geophysics 10, 339-349.

Gibbard, P.L., 1982. Terrace stratigraphy and drainage history of the plateau gravels of north Surrey, south Berkshire, and north Hampshire, England. Proceedings of the Geologists' Association 93, 369-384.

Gomme, J., Buss, S., 2006. Groundwater Quality Review: Thames Valley Gravels, Thames Region. Environment Agency Report 6441R8, Reading, UK.

Green, C.P., Coope, G.R., Jones, R.L., Keen, D.H., Bowen, D.Q., Currant, A.P., Holyoak, D.T., Ivanovich, M., Robinson, J.E., Rogerson, R.J., Young, R.C., 1996. Pleistocene deposits at Stoke Goldington, in the valley of the Great Ouse, UK. Journal of Quaternary Science 11, 59-87.

Guccione, M.J., 2008. Impact of the alluvial style on the geoarcheology of stream valleys. Geomorphology 101, 378-401.

Hickin, A.S., Kerr, B., Barchyn, T.E., Paulen, R.C., 2009. Using ground-penetrating radar and capacitively coupled resistivity to investigate 3-D fluvial architecture and grain-size distribution of a gravel floodplain in northeast British Columbia, Canada. Journal of Sedimentary Research 79, 457-477.

Hill, I., Jeffrey, C.A., Hameed, A., 2011. Geophysical Quality Assessment of Sand and Gravel Deposits. Proceedings of Near Surface 2011, European Association of Geoscientists and Engineerings, University of Leicester, UK.

Hirsch, M., Bentley, L.R., Dietrich, P., 2008. A comparison of electrical resistivity, ground penetrating radar and seismic refraction results at a river terrace site. Journal of Environmental and Engineering Geophysics 13, 325-333.

Horton, A., 1970. The Drift Sequence and Sub-glacial Topography in Parts of the Ouse and Nene Basins. Report of the Institute of Geological Sciences 70/9. HMSO, London.

Hsu, H.L., Yanites, B.J., Chen, C.C., Chen, Y.G., 2010. Bedrock detection using 2D electrical resistivity imaging along the Peikang River, central Taiwan. Geomorphology 114, 406-414.

Jeffrey, C., Hill, I., Hameed, A, 2011. Deposit Knowledge for Efficient Production. Defra, Mineral Industry Sustainable Technology Fund, Commissioned Report MA/7/G/002, University of Leicester, UK.

Loke, M.H., Barker, R.D., 1996. Practical techniques for 3D resistivity surveys and data inversion. Geophysical Prospecting 44, 499-523.

Loke, M.H., Acworth, I., Dahlin, T., 2003. A comparison of smooth and blocky inversion methods in 2D electrical imaging surveys. Exploration Geophysics 34, 182-187.

Magnusson, M.K., Fernlund, J.M.R., Dahlin, T., 2010. Geoelectrical imaging in the interpretation of geological conditions affecting quarry operations. Bulletin of Engineering Geology and the Environment 69, 465-486.

Marr, D., Hildreth, E., 1980. Theory of edge-detection. Proceedings of the Royal Society of London Series B-Biological Sciences 207, 187-217.

Merritt, J.W., 1992. A critical-review of methods used in the appraisal of onshore sand and gravel resources in Britain. Engineering Geology 32, 1-9.

Peterson, C.D., Minor, R., Peterson, G.L., Gates, E.B., 2011. Pre and post-Missoula flood geomorphology of the pre-Holocene ancestral Columbia River valley in the Portland forearc basin, Oregon and Washington, USA. Geomorphology 129, 276-293.

Revil, A., Cary, L., Fan, Q., Finizola, A., Trolard, F., 2005. Self-potential signals associated with preferential ground water flow pathways in a buried paleo-channel. Geophysical Research Letters 32, L07401.

Rogerson, R.J., Keen, D.H., Coope, G.R., Robinson, E., Dickson, J.H., Dickson, C.A., 1992. The fauna, flora and palaeoenvironmental significance of deposits beneath the low terrace of the River Great Ouse at Radwell, Bedfordshire, England. Proceedings of the Geologists' Association 103, 1-13.

Rowan, T., 1990. Functional stability analysis of numerical algorithms. Ph.D. thesis, Department of Computer Sciences, University of Texas at Austin.

Sass, O., 2007. Bedrock detection and talus thickness assessment in the European Alps using geophysical methods. Journal of Applied Geophysics 62, 254-269.

Sheather, S.J., Jones, M.C., 1991. A reliable data-based bandwidth selection method for kernel density estimation. Journal of the Royal Statistical Society B 53, 683–690.

Shevnin, V., Mousatov, A., Ryjov, A., Delgado-Rodriquez, O., 2007. Estimation of clay content in soil based on resistivity modelling and laboratory measurements. Geophysical Prospecting 55, 265-275.

Sjodahl, P., Dahlin, T., Zhou, B., 2006. 2.5D resistivity modeling of embankment dams to assess influence from geometry and material properties. Geophysics 71, G107-G114.

Smith, M.R., Collis, L., 2001. Aggregates: Sand, Gravel and Crushed Rock Aggregates for Construction Purposes. The Geological Society, London.

Suzuki, R., Hiyama, T., Asanuma, J., Ohata, T., 2004. Land surface identification near Yakutsk in eastern Siberia using video images taken from a hedgehopping aircraft. International Journal of Remote Sensing 25, 4015-4028.

Tye, A.M., Kessler, H., Ambrose, K., Williams, J.D.O., Tragheim, D., Scheib, A., Raines, M., Kuras, O., 2011. Using integrated near-surface geophysical surveys to aid mapping and interpretation of geology in an alluvial landscape within a 3D soil-geology framework. Near Surface Geophysics 9, 15-31.

Vafidis, A., Economou, N., Ganiatsos, Y., Manakou, M., Poulioudis, G., Sourlas, G., Vrontaki, E., Sarris, A., Guy, M., Kalpaxis, T., 2005. Integrated geophysical studies at ancient Itanos (Greece). Journal of Archaeological Science 32, 1023-1036.

Wardrop, D.R., 1999. A study on the accuracy of sand and gravel reserve estimates. Quarterly Journal of Engineering Geology 32, 81-86.

Wilkinson, P.B., Loke, M.H., Meldrum, P.I., Chambers, J.E., Kuras, O., Gunn, D.A., and Ogilvy, R.D., 2012. Practical aspects of applied optimised survey design for Electrical Resistivity Tomography. Geophysical Journal International 189, 428-440.

Wymer, J., 1988. Paleolithic archaeology and the British Quaternary sequence. Quaternary Science Reviews 7, 79-98.

List of Figures

Fig. 1. Geological map based on a recent geological resurvey of the area (Barron et al., 2010), showing the location of the study site and the distribution of artificially modified ground associated with extractive activities. Coordinate systems are given as longitude and latitude (bold) and British National Grid (normal). Inset map (top left) shows the location of the study site within the UK.

Fig. 2. Three-dimensional ERT survey area (red shading), site boundary (black line), and line locations (red lines, 6-m separation), and borehole positions (black dots). Banked topsoil stockpiles (grey shading) crest heights are typically 3 m above ground level.

Fig. 3. Example of a resistivity depth curve (black line) generated from PCHIP interpolation of resistivity data (circles) and the gradient (first derivative) of the resistivity (grey line). The maximum positive gradient is shown by the dashed black line.

Fig. 4. Three-dimensional ERT model displayed as (A) a solid volume, (B) a solid volume with opaque volume defining resistivities above 200 Ωm, (C) vertical sections, (D) a horizontal section at 20 m AOD. Vertical extent of mineral and overburden, determined from drilling, shown as grey cylinders. The southeastern edge of the incised channel structure is indicated as a dashed white line.

Fig. 5. Probability distribution plot of the Willington 3D ERT data (solid line), and optimised probability distribution model (dashed line) for three normal distributions with peaks at log resistivities of 1.21, 1.75, and 2.09 Ωm (i.e., resistivities of 16, 56, and 123 Ωm).

Fig. 6. Resistivity data (circles) and interpolating curves (blue line) as a function of elevation, given as mAOD at surface positions corresponding to BH11 (top) and BH15 (bottom). The elevations associated with the steepest gradient method (SGM) and the intersections between the borehole-derived elevations and the resistivity depth curves (interface resistivities) are indicated. Drilling results for four different techniques at this location are shown: flight auger (FA); shell and auger (SA); reverse circulation (RC); sonic (SNC).

Fig. 7. Bedrock surface determined using the steepest gradient (first derivative) method, showing the erosional structure associated with the transition from the first to the second terrace of the Great Ouse.

Fig. 8. (A) Bland Altman plot of steepest gradient method and borehole-derived (BH) elevations, showing the 95% confidence limit between -0.56 and 0.93 m. (B) Cross plot of steepest gradient method and borehole-derived bedrock elevations, showing Pearson correlation coefficient.

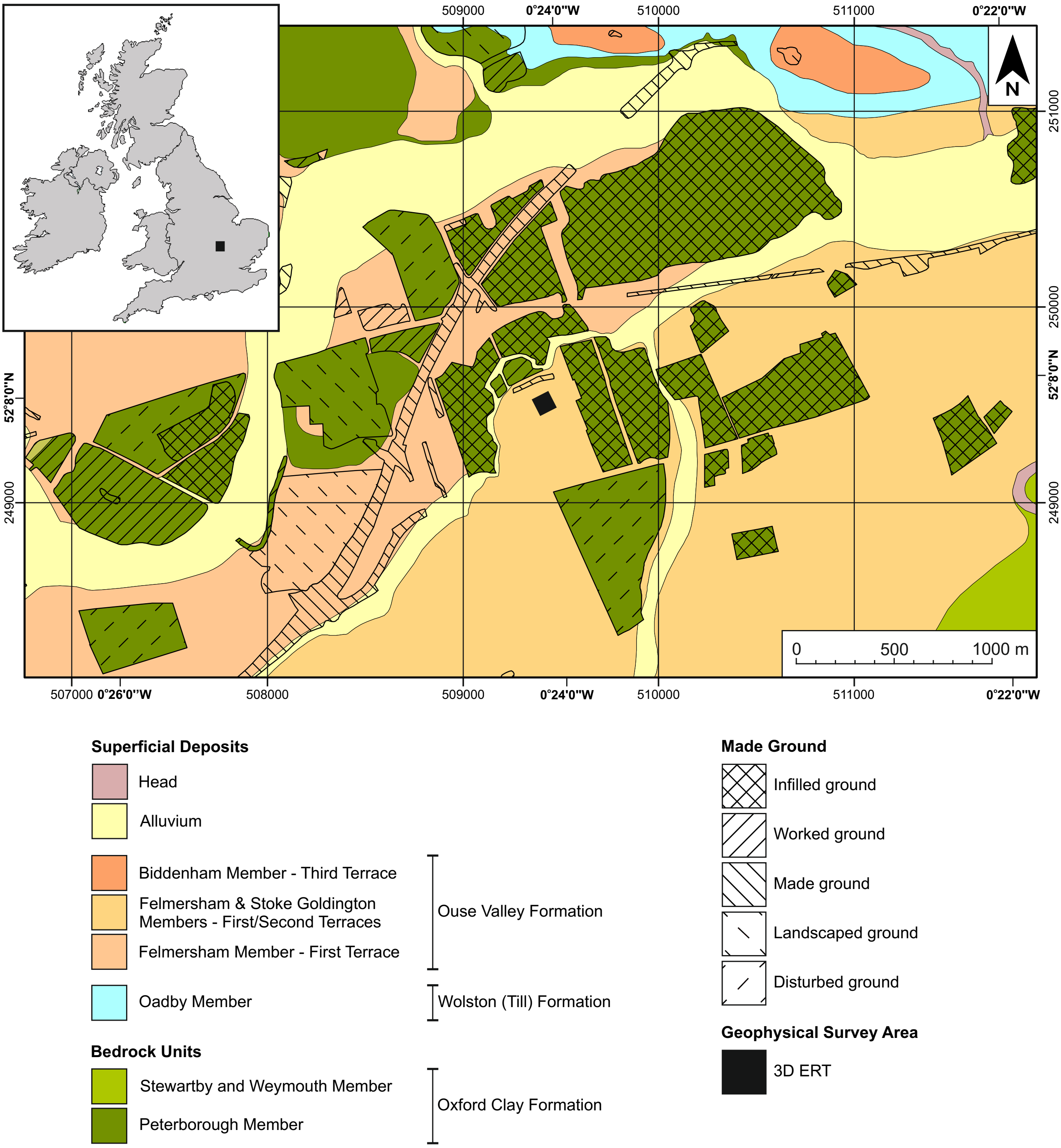

509000
0°24'0"W
510000
511000
0°22'0"W
N
251000
250000
52°8'0"N
249000
0 500 1000 m
507000 0°26'0"W
508000
Superficial Deposits
Head
Alluvium
Biddenham Member - Third Terrace
Felmersham & Stoke Goldington Members - First/Second Terraces
Felmersham Member - First Terrace
Ouse Valley Formation
Oadby Member
Wolston (Till) Formation
Bedrock Units
Stewartby and Weymouth Member
Peterborough Member
Oxford Clay Formation
Made Ground
Infilled ground
Worked ground
Made ground
Landscaped ground
Disturbed ground
Geophysical Survey Area
3D ERT

Figure 1

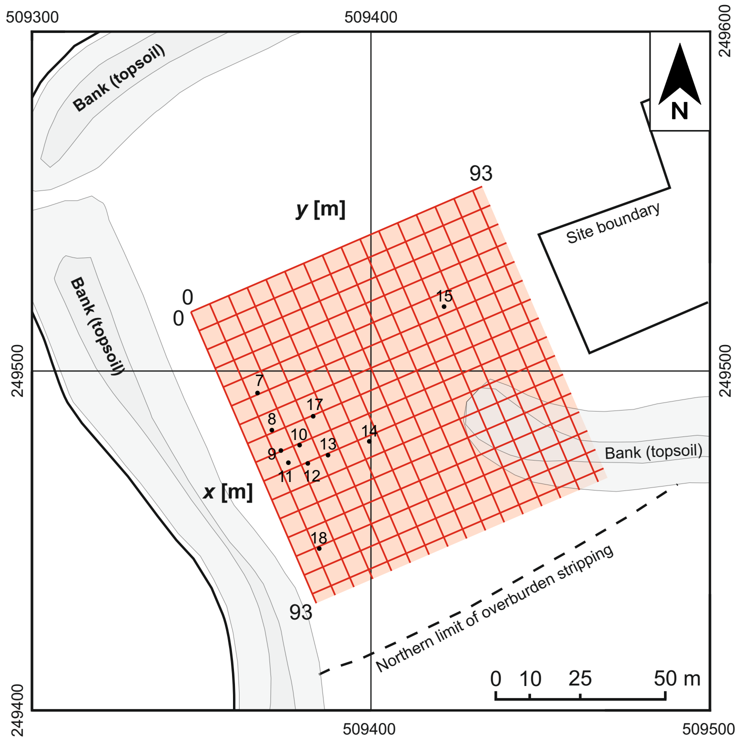
509300
509400
249600
Bank (topsoil)
N
93
y [m]
Site boundary
0
0
15
Bank (topsoil)
249500
249500
7
17
8
10
14
9
13
11
12
Bank (topsoil)
x [m]
18
93
Northern limit of overburden stripping
0 10 25 50 m
249400
509400
509500

Figure 2

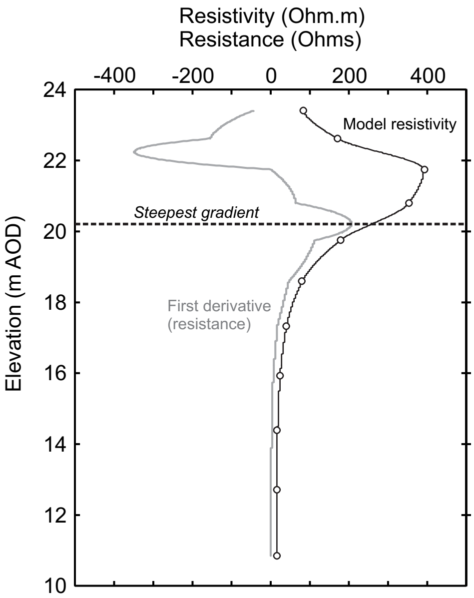
Resistivity (Ohm.m)
Resistance (Ohms)
-400
-200
0
200
400
24
22
20
18
16
14
12
10
Elevation (m AOD)
Model resistivity
Steepest gradient
First derivative
(resistance)

Figure 3

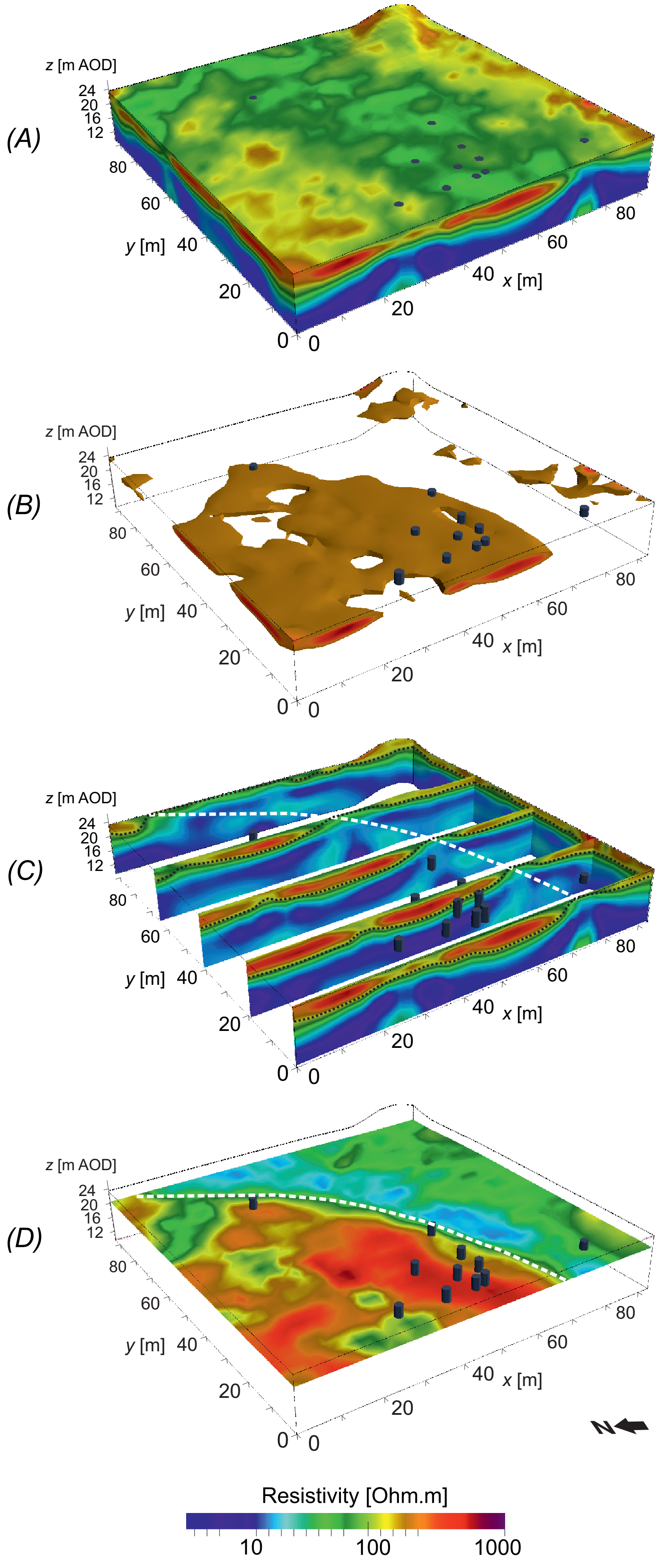
(A)
(B)
(C)
(D)
z [m AOD]
24
20
16
12
y [m]
x [m]
0
20
40
60
80
N
Resistivity [Ohm.m]
10
100
1000

Figure 4

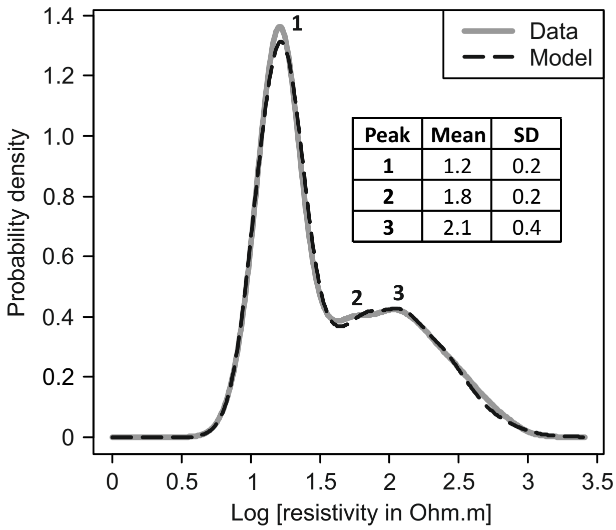
1.4
1.2
1.0
0.8
0.6
0.4
0.2
0
Probability density
0
0.5
1
1.5
2
2.5
3
3.5
Log [resistivity in Ohm.m]
Data
Model
1
2
3
Peak | Mean | SD
1 | 1.2 | 0.2
2 | 1.8 | 0.2
3 | 2.1 | 0.4

Figure 5

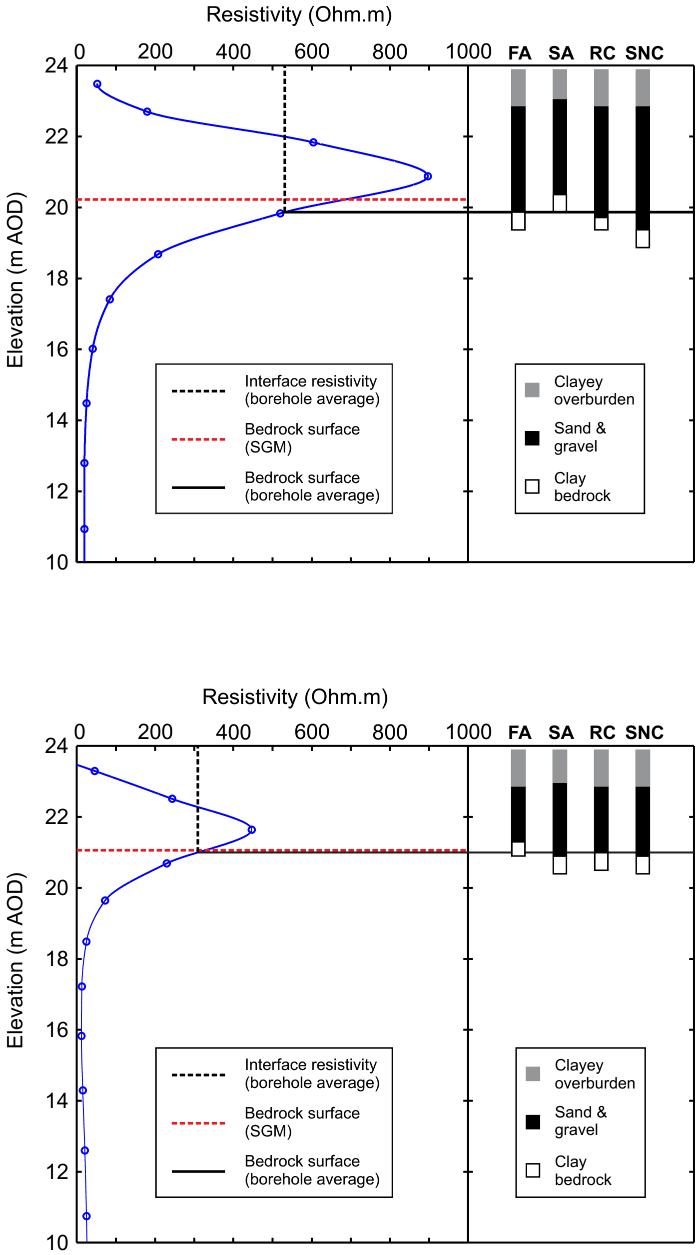
Resistivity (Ohm.m)
0
200
400
600
800
1000
FA
SA
RC
SNC
24
22
20
18
16
14
12
10
Elevation (m AOD)
Interface resistivity (borehole average)
Bedrock surface (SGM)
Bedrock surface (borehole average)
Clayey overburden
Sand & gravel
Clay bedrock
Resistivity (Ohm.m)
0
200
400
600
800
1000
FA
SA
RC
SNC
24
22
20
18
16
14
12
10
Elevation (m AOD)
Interface resistivity (borehole average)
Bedrock surface (SGM)
Bedrock surface (borehole average)
Clayey overburden
Sand & gravel
Clay bedrock

Figure 6

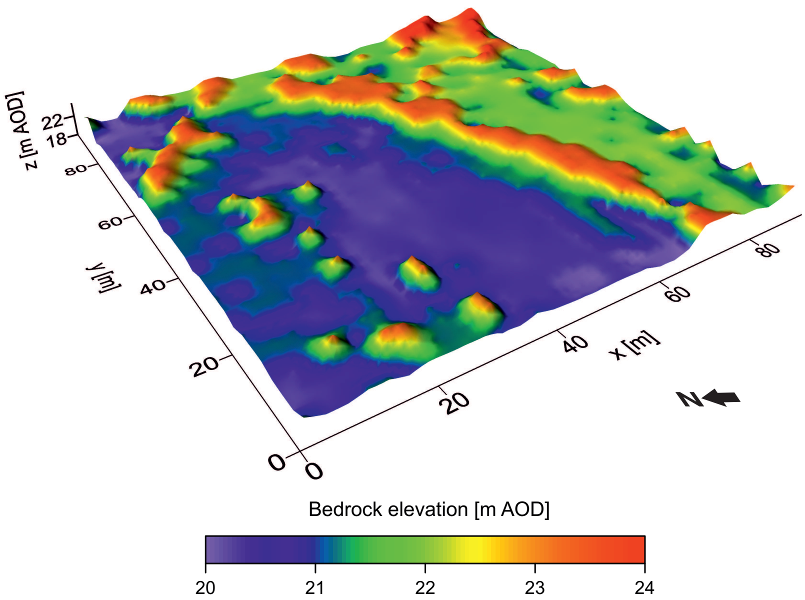
z [m AOD]
22
18
80
60
y [m]
40
20
0
0
20
40
x [m]
60
80
N
Bedrock elevation [m AOD]
20
21
22
23
24

Figure 7

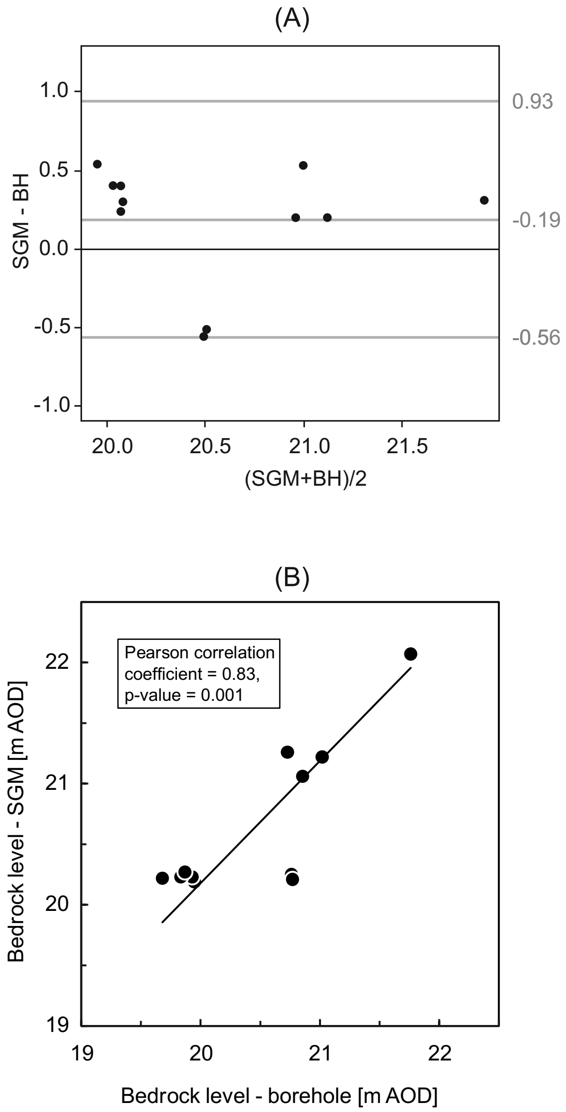
(A)
1.0
0.5
0.0
-0.5
-1.0
SGM - BH
0.93
-0.19
-0.56
20.0
20.5
21.0
21.5
(SGM+BH)/2
(B)
Pearson correlation
coefficient = 0.83,
p-value = 0.001
22
21
20
19
Bedrock level - SGM [m AOD]
19
20
21
22
Bedrock level - borehole [m AOD]

Figure 8